

Role of left-hand cut contributions on pole extractions from lattice data: Case study for $T_{cc}(3875)^+$

Meng-Lin Du¹, Arseniy Filin², Vadim Baru², Xiang-Kun Dong^{3,4}, Evgeny Epelbaum²,
Feng-Kun Guo^{3,4,5}, Christoph Hanhart⁶, Alexey Nefediev^{7,8}, Juan Nieves⁹, and Qian Wang^{10,11,12}

¹*School of Physics, University of Electronic Science and Technology of China, Chengdu 611731, China*

²*Institut für Theoretische Physik II, Ruhr-Universität Bochum, D-44780 Bochum, Germany*

³*CAS Key Laboratory of Theoretical Physics, Institute of Theoretical Physics,
Chinese Academy of Sciences, Beijing 100190, China*

⁴*School of Physical Sciences, University of Chinese Academy of Sciences, Beijing 100049, China*

⁵*Peng Huanwu Collaborative Center for Research and Education, Beihang University, Beijing 100191, China*

⁶*Institute for Advanced Simulation, Institut für Kernphysik and Jülich Center
for Hadron Physics, Forschungszentrum Jülich, D-52425 Jülich, Germany*

⁷*Jozef Stefan Institute, Jamova 39, 1000 Ljubljana, Slovenia*

⁸*CeFEMA, Center of Physics and Engineering of Advanced Materials,
Instituto Superior Técnico, Avenida Rovisco Pais 1, 1049-001 Lisboa, Portugal*

⁹*Instituto de Física Corpuscular (centro mixto CSIC-UV),
Institutos de Investigación de Paterna, Apartado 22085, 46071, Valencia, Spain*

¹⁰*Guangdong Provincial Key Laboratory of Nuclear Science, Institute of
Quantum Matter, South China Normal University, Guangzhou 510006, China*

¹¹*Institute of High Energy Physics, Chinese Academy of Sciences, Beijing 100049, China*

¹²*Guangdong-Hong Kong Joint Laboratory of Quantum Matter, Southern Nuclear
Science Computing Center, South China Normal University, Guangzhou 510006, China*

We discuss recent lattice data for the $T_{cc}(3875)^+$ state to stress a potentially strong impact of left-hand cuts from the one-pion exchange on the pole extraction for near-threshold states. In particular, if the left-hand cut is located close to the two-particle threshold, which happens naturally in the DD^* system for the pion mass exceeding its physical value, the effective-range expansion is valid only in the very limited energy range up to the cut and as such is of little use to reliably extract the poles. Then, an accurate extraction of the pole locations requires the one-pion exchange to be implemented explicitly into the scattering amplitudes.

I. INTRODUCTION

The last two decades have witnessed the discovery of a large number of the so-called exotic hadronic states in the heavy quark sector that do not fit into the scheme of simple quark models [1–9]. In some cases, only particular properties of such states like masses or decays strongly deviate from expectations. However, the quantum numbers of some others unambiguously indicate their multi-quark content—the most prominent representatives of this class are the isotriplet Z_c and Z_b states that decay, for example, to a heavy quarkonium plus a single pion. For an overview of the experimental situation see, for example, Ref. [7]. The pressing theoretical question is what clusters the quarks form in these exotic hadrons, if any. One popular scenario is that diquarks and anti-diquarks emerge as relatively compact building blocks carrying a color charge [1, 2]. Then, if there are light quarks in the system, the size of the emerging states should be governed by the confinement radius, $\sim 1/\Lambda_{\text{QCD}}$, with $\Lambda_{\text{QCD}} \sim 300$ MeV. Such a size does not depend on the binding energy E_b defined as the difference between the mass of the state and the energy of the closest threshold. Alternatively, the building blocks could be color-neutral conventional hadrons. Then, the size of these so-called hadronic molecules is given by the inverse of the binding momentum $\gamma = \sqrt{2\mu E_b} \ll \Lambda_{\text{QCD}}$, with μ for the

reduced mass, resulting in large radii of near-threshold states. Thus, the size of hadronic molecules is limited by the binding momentum rather than by the structure of the interaction. This difference in size leads to significant differences in some observables [4]. Because of confinement, only multi-hadron intermediate states, being color singlets, can be on-shell thereby generating a unitarity or right-hand cut (rhc) in the amplitude. The argument can be further generalized to unstable constituents [10, 11], as long as they are not too broad [12], meaning their life time is still larger than the range of forces [13].

For concreteness, we present our findings with the focus on the double-charm meson state T_{cc}^+ reported in Refs. [14, 15] and treated in this work as a DD^* molecule. Among many exotic candidates, the T_{cc}^+ is of a particular interest since its width, apart from a tiny electromagnetic contribution, stems almost entirely from the only available strong decay channel $DD\pi$, as a consequence of the finite D^* life time. Then, the only relevant cut of the amplitude on the real axis is the three-body $DD\pi$ cut indicated as the vertical blue dashed lines in Fig. 1, while the DD^* branch cut, shown in the same figure as the green dashed vertical line, splits into a pair of cuts on the second sheet in the complex energy plane [16, 17]. The branch point of the $DD\pi$ cut is located below the nominal DD^* threshold.

The cut structure of the amplitude severely changes

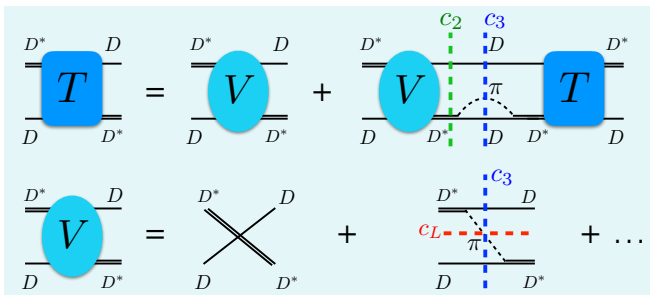


FIG. 1. The cut structure in the DD^* system: (i) the blue dotted vertical lines (c_3) indicate the three-body right-hand cuts, (ii) the green dotted vertical line (c_2) shows the two-body cut, and (iii) the red dotted horizontal line (c_L) is for the left-hand cut. Here T and V denote the amplitude and interaction potential, respectively. All lines in the diagrams are labeled explicitly.

for a heavier pion, which can be studied using lattice QCD and chiral effective field theories. As soon as the pion mass exceeds the D^*-D mass difference, the T_{cc}^+ is stable with respect to the strong interaction, the $DD\pi$ three-body cut branch point appears above the DD^* two-body threshold, and the pion exchange induces the so-called left-hand cut (lhc), indicated as the red dashed horizontal line in Fig. 1, that is in the spotlight of this work. Since the location of its branch point is related to the range of the potential and the discontinuity depends on its strength, the cut is also called dynamical [18].

Lattice QCD studies of the T_{cc}^+ have been recently performed in Refs. [19–21]. The last work employs the method developed by the HAL QCD Collaboration to extract the DD^* scattering potential first and then use it to calculate the phase shifts above the two-body threshold. The consideration presented in this Letter does not directly apply to this approach. In the first two works the Lüscher method is employed to extract the DD^* phase shifts $\delta(E)$ at $m_\pi = 280$ and 350 MeV, respectively. Meanwhile, in Ref. [20], there is only one data point in the near-threshold region and only a single lattice volume is investigated, so the authors themselves argue that a proper discussion of the pole structure of the amplitude is not possible yet. Therefore, in our study we stick to the phase shifts extracted from the lattice calculations of Ref. [19]. These phase shifts are related to the scattering T -matrix as

$$-\frac{2\pi}{\mu}T^{-1}(E) = p \cot \delta - ip, \quad (1)$$

with E and p the energy and the magnitude of the relative momentum in the center-of-mass (c.m.) frame, respectively, and a pole of the T -matrix appears, if

$$p \cot \delta = ip. \quad (2)$$

To exploit the latter condition, the phase shifts ex-

tracted from the lattice calculations were parameterized retaining the first two terms in the effective range expansion (ERE)¹,

$$p \cot \delta = \frac{1}{a} + \frac{1}{2}rp^2 + \mathcal{O}(p^4), \quad (3)$$

where a and r are the scattering length and effective range, respectively. However, the radius of convergence of the ERE is set by the location of the nearest singularity irrespective of its origin. In this Letter we argue that, in the settings of Ref. [19], the physics related to the lhc is relevant and cannot be ignored. In particular, we demonstrate that, in the vicinity of the lhc, the simple approximation (3) has to be abandoned in favor of the exact solution of the dynamical equation in the presence of pions (see Fig. 1), which has a strong effect on both $p \cot \delta$ and the extracted pole. Thus, the physics discussed in this Letter is related to the left-hand cuts of the long-range potentials and is quite general.

We also emphasize that the phase shifts extracted from the lattice data and employed in our analysis may need to be revisited in the future. In particular, the presence of the lhc requires a modification of the Lüscher method [24] and may induce sizable partial-wave mixing effects [25]. Being unable to estimate quantitatively the importance of these effects, we take the phase shifts extracted above the lhc for granted.

II. CUT STRUCTURE OF THE DD^* AMPLITUDE

In line with the available lattice setting employed to analyze the DD^* system, we work in the isospin limit. Then the $T_{cc}(3875)^+$ is a purely isoscalar state. The relevant degrees of freedom for its description are DD^* and $DD\pi$, introducing two- and three-body branch points in the amplitude, respectively. For the physical pion mass, pions contribute to the DD^* dynamics in two ways: through the D^* selfenergy and the DD^* scattering potential. Both induce right-hand cuts to the amplitude—see the upper and lower blue dashed vertical lines in Fig. 1, respectively. The three-body $DD\pi$ Green’s function, which generates the most relevant cut in the DD^* scattering amplitude (see the left plot in Fig. 2),² reads [26–29]

$$\begin{aligned} G_\pi^{-1}(E, \mathbf{k}', \mathbf{k}) &= E - E_D(k^2) - E_D(k'^2) - \omega_\pi(q^2) \\ &\approx E - 2M_D - \frac{k^2 + k'^2}{2M_D} - \omega_\pi(q^2), \end{aligned} \quad (4)$$

¹ If one of the scattering particles is unstable, it is convenient to make the ERE around the complex branch point connected to the two-body channels [22, 23].

² There is in addition the $D^*D^*\pi$ Green’s function (see Eq. (A2) in the appendix and the right plot in Fig. 2), which is, however, irrelevant for this discussion.

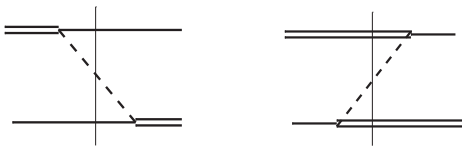


FIG. 2. The two contributions to the OPE interaction between the D^* (double solid line) and D (single solid line) mesons; the dashed line corresponds to the pion. The thin vertical line picks up the relevant intermediate state: $DD\pi$ and $D^*D^*\pi$ for the left and right plot, respectively.

where E denotes the total energy, \mathbf{k} (\mathbf{k}') is the incoming (outgoing) DD^* relative momentum in the overall c.m. system, $E_D(k) = \sqrt{M_D^2 + k^2}$ and $k(k')$ is the corresponding magnitude. The pion energy in the intermediate state is $\omega_\pi(q^2) = \sqrt{m_\pi^2 + q^2}$, with $\mathbf{q} = \mathbf{k} - \mathbf{k}'$ and $q = |\mathbf{q}|$. Since isospin breaking effects are not taken into account in the lattice calculations, we use isospin averaged masses for all mesons.

For the physical pion mass, $m_\pi < \Delta M \equiv M_{D^*} - M_D$, and one can find real values of k and k' such that $G_\pi^{-1} = 0$ for each energy E above the three-body threshold $E_{\text{thr}} \equiv 2M_D + m_\pi$, with the interpretation of the $DD\pi$ state going on-shell. At the same time, the DD^* Green's function has two branch points in the complex s plane ($s = E^2$), giving rise to the two-body unitarity cuts in the scattering amplitude. This situation is sketched in Fig. 3 (b) together with the pole locations for the T_{cc}^+ .

If we now increase the pion mass, ΔM will change only very little (it is governed by the heavy-quark spin symmetry violation and not by chiral dynamics), but the phase space for the $DD\pi$ state will shrink. For $m_\pi > \Delta M$, D^* becomes stable (we neglect its possible radiative decays that are not considered in lattice calculations either), and the DD^* branch cut moves to the real axis. In this setting we measure the energy relative to the DD^* threshold to write $E = M_{D^*} + M_D + p^2/(2\mu)$, where $\mu = M_{D^*}M_D/(M_{D^*} + M_D)$. Then

$$G_\pi^{-1}(E, \mathbf{k}', \mathbf{k}) = \Delta M + \frac{p^2}{2\mu} - \frac{k^2 + k'^2}{2M_D} - \omega_\pi(q^2). \quad (5)$$

The two-body branch point is now located at $E_{DD^*} = M_D + M_{D^*}$, which implies

$$p_{\text{rhc}_2}^2 = 0. \quad (6)$$

The three-body branch point can be found by setting $k = k' = 0$ to be

$$p_{\text{rhc}_3}^2 = 2\mu(m_\pi - \Delta M). \quad (7)$$

In addition, new singularities emerge from Eq. (5) in the on-shell partial-wave amplitudes at imaginary values of the momenta, $k^2 = k'^2 = p^2 < 0$. Using that $\mu \approx M_D/2$, the smallest in magnitude value of p^2 where this happens

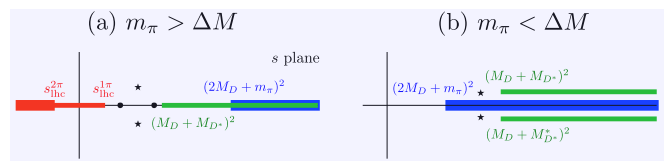


FIG. 3. Sketch of the locations of various branch cuts in the complex s -plane: (a) for $m_\pi = 280$ MeV and (b) for the physical pion mass. The left-hand, two-body DD^* , and three-body $DD\pi$ cuts are shown in red, green, and blue, respectively. The black symbols show typical locations for the T_{cc}^+ poles: they can correspond to a pair of virtual states (dots) or a resonance (stars) in case (a) and to a quasi-bound state in case (b).

is given by $\omega_\pi(4p^2) \approx \Delta M$ (backward scattering), so that

$$(p_{\text{lhc}}^{1\pi})^2 \approx \frac{1}{4}(\Delta M^2 - m_\pi^2). \quad (8)$$

This sets the location of the branch point that leads to the lhc nearest to the threshold. In principle, there are additional lhc's from two or more pion exchanges or the exchange of heavier mesons. Those, however, are not relevant to the discussion here. The cut structure in the complex s plane for $m_\pi > \Delta M$ is shown in Fig. 3 (a). An lhc introduces nonanalyticity to $p \cot \delta$ defined in Eq. (1) and, accordingly, sets the upper bound for the convergence radius of the ERE introduced in Eq. (3). For the case at hand, $p \cot \delta$ acquires an imaginary part for energies below the lhc and, therefore, can not be treated as real-valued.

III. RESULTS AND DISCUSSION

For an illustration of the general concept, in this Letter we focus on the lattice data from Ref. [19] collected at $m_\pi = 280$ MeV, $M_D = 1927$ MeV and $M_{D^*} = 2049$ MeV (the second data set for the smaller charm quark mass provided in Ref. [19] leads to quite analogous results – see Appendix B). Then with $\Delta M = 122$ MeV $< m_\pi$ we find

$$(p_{\text{lhc}}^{1\pi})^2 = -(126 \text{ MeV})^2 \implies \left(\frac{p_{\text{lhc}}^{1\pi}}{E_{DD^*}} \right)^2 = -0.001, \quad (9)$$

where $E_{DD^*} = M_D + M_{D^*}$. In Fig. 4 the location of this lhc branch point is indicated with the vertical dashed line. The $DD\pi$ rhc branch point is now located far away, at

$$p_{\text{rhc}_3}^2 = (552 \text{ MeV})^2 \implies \left(\frac{p_{\text{rhc}_3}}{E_{DD^*}} \right)^2 = +0.02, \quad (10)$$

and is irrelevant for the analysis of these lattice data (see the abscissa axis range in Fig. 4).

In Ref. [19] the lattice data were analyzed to extract the location of the T -matrix pole using a linear (in p^2)

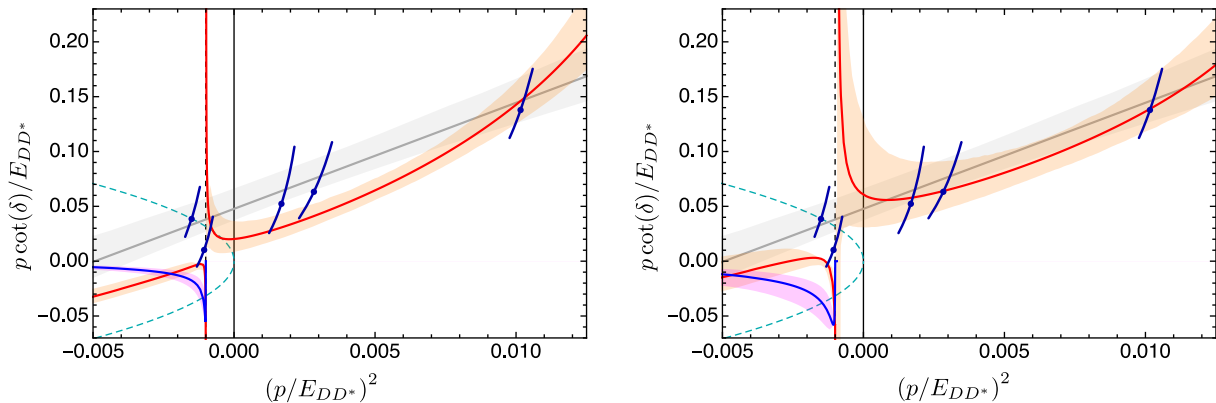


FIG. 4. Fit results for the lattice data from Ref. [19]. The solid and dashed vertical lines indicate the DD^* threshold and the lhc, respectively, while the green dashed curve shows the function ip . The gray line and gray band show the fit and its 1σ uncertainty, respectively, found in Ref. [19] using the ERE formula from Eq. (3) in the entire energy range both above and below lhc. The red solid line and the orange band show the best fit and its 1σ uncertainty, respectively, calculated in this work. In the second plot (right panel) only the three most right data points were used in the fit while in the first plot (left panel), in addition, a part of the error bar of the fourth (from right to left) point that is located above the left-hand cut (i.e. for $(p/E_{DD^*})^2 > -0.001$) is included in the fit. Below the lhc, $p \cot \delta$ acquires an imaginary part, which is shown as the blue line with the pink uncertainty band.

fit, as defined in Eq. (3), in the full energy range, thereby yielding a pole location at $p^2/(2\mu) = -9.9$ MeV, on the second Riemann sheet of the complex s plane, which translates to $(p/E_{DD^*})^2 = -0.001$. In Fig. 4 this fit is shown as the gray line including its 1σ uncertainty band shown in light gray. Thus, the pole extracted using only the first two terms in the ERE is located at the lhc or even below it. However, since the lhc sets the radius of convergence of the ERE, the latter is only valid in a small range $|(p/E_{DD^*})^2| \ll 0.001$, in which no lattice data exist. Furthermore, the central values of the two data points crucial for the fit performed in Ref. [19] lie below the lhc, though in this case $p \cot \delta$ becomes complex. Therefore, this pole extraction procedure cannot be regarded as reliable.

To improve on the extraction of the pole parameters from the phase shifts of Ref. [19] we fit the lattice data with an amplitude that includes the lhc.³ More precisely, we solve the DD^* scattering equation employing a potential that incorporates the one-pion exchange and two contact terms—one momentum-independent and one momentum-dependent. The latter are treated as two fitting parameters. This is a simplified version of the full amplitude of Ref. [29], where all D waves are now switched off to be in line with Ref. [19]. The chiral extrapolation of the involved pion decay constant is considered using chiral perturbation theory [32] and that of the $D^*D\pi$ coupling is taken from Ref. [33, 34]. Further

details of the framework and fitting procedure are provided in Appendix A. The results of this procedure are shown in Fig. 4 as the red line with the orange uncertainty band.⁴ We did not include the lowest data point in the fit, since it lies below the lhc and was extracted with a formula that ignores it. Since a part of the uncertainty range of the second data point extends to the energy range above the lhc, we performed two fits: one with this part included in the fit (the left panel of Fig. 4) and the other one where we ignored it (the right panel of Fig. 4). The upper three data points were included in both fits.

The poles of the T -matrix can now be extracted using Eq. (2), which can be illustrated graphically as an intersection of the orange band with the green dashed curve from unitarity. We, therefore, conclude from the results presented in the left panel of Fig. 4 that for the majority of the 1σ parameter space, including the best fit, the amplitude contains two virtual states, both residing closer to the DD^* threshold than the pole extracted in the original analysis of Ref. [19], where only a single virtual state was found. Those fits within the 1σ band, where $p \cot \delta$ does not cross the ip curve above the lhc, describe the presence of a very narrow resonance that shows up as a pair of complex poles below the DD^* threshold. The appearance of a pair of virtual states is indeed natural near the point where they are about to turn to a narrow

³ An important role played by the lhc from pion exchanges for NN scattering at unphysical pion masses was pointed out in Refs. [30, 31].

⁴ Since the three-body cut is sufficiently far away, see Eq. (10), the D -meson recoil terms can be neglected. While the results shown in Fig. 4 were obtained with the recoil corrections included, we checked that their impact on the results is negligible.

resonance, as discussed in detail in Ref. [35–38]. One also concludes that, *inter alia*, the position of the lhc sets the upper bound on the virtual pole binding energy—the collision between the virtual pole and its counterpart that appears from under the lhc always takes place between the lhc branch point and the two-body threshold. The fit results presented in the right panel of Fig. 4 are also consistent with the picture just drawn, with the narrow resonance scenario preferred.

Both fits provide parameter sets such that $p \cot \delta$ contains a pole as a result of a subtle interplay of the repulsive one-pion exchange and the attractive short-range interactions. According to Eq. (1), this pole manifests itself as a zero in the T -matrix and provides yet another illustration that, in the current setting, $p \cot \delta$ cannot be approximated by a polynomial with a finite number of terms. Moreover, it emphasizes the important role played by the one-pion exchange for the problem at hand.

IV. CONCLUDING REMARKS

An interesting question is what our findings on the pole location imply for the nature of the T_{cc}^+ —after all there is an intriguing relationship between the location of the pole connected to a near-threshold bound state and the size of its molecular component—see Refs. [39, 40] (the equivalence between the two approaches was discussed first in Ref. [41]). The generalization of these ideas to virtual states is provided in Ref. [42] and for a positive effective range, which is the case for the lattice analyses of T_{cc}^+ [19, 20], in Refs. [43, 44]. However, it must be stressed that the formalism quoted above relies on the assumption that the binding momentum γ is by far the smallest scale in the problem. Here, however, the lhc induces an additional small scale, which not only strongly limits the range of applicability of the ERE (for a related discussion, see Ref. [28]), but also calls for an improvement of the entire Weinberg approach to describe the

compositeness of a hadronic state.⁵ On the other hand, a clear visibility in the amplitude of the lhc induced by the one-pion exchange provides an additional strong support for the molecular nature of the $T_{cc}(3875)^+$.

In summary, we have demonstrated that the left-hand cuts from the long-range interactions, with the nearest one originating from the one-pion exchange, strongly restrict the range of validity for the effective-range expansion used in lattice simulations to extract the pole positions of near-threshold states. In order to increase this range and thereby extract the poles reliably, at least the one-pion exchange needs to be taken into account explicitly. The described feature is general, and we illustrated this by reanalyzing the lattice data of Ref. [19] for the $T_{cc}(3875)^+$ state.

ACKNOWLEDGMENTS

The authors would like to thank Sasa Prelovsek for reading the manuscript and valuable comments. This work is supported in part by the National Natural Science Foundation of China (NSFC) and the Deutsche Forschungsgemeinschaft (DFG) through the funds provided to the Sino-German Collaborative Research Center TRR110 “Symmetries and the Emergence of Structure in QCD” (NSFC Grant No. 12070131001, DFG Project-ID 196253076); by the Chinese Academy of Sciences under Grant No. XDB34030000; by the NSFC under Grants No. 12125507, No. 11835015, and No. 12047503; by the EU STRONG-2020 project under the program H2020-INFRAIA-2018-1 with Grant No. 824093; by the Spanish Ministerio de Ciencia e Innovación (MICINN) under Grant No. PID2020-112777GB-I00; by Generalitat Valenciana under Grant PROMETEO/2020/023; by BMBF (Contract No. 05P21PCFP1) and by the MKW NRW under the funding code NW21-024-A. A.N. is supported by the Slovenian Research Agency (research core Funding No. P1-0035). Q.W. is also supported by Guangdong Provincial funding with Grant No. 2019QN01X172.

-
- [1] A. Esposito, A. L. Guerrieri, F. Piccinini, A. Pilloni, and A. D. Polosa, *Int. J. Mod. Phys. A* **30**, 1530002 (2015).
 - [2] R. F. Lebed, R. E. Mitchell, and E. S. Swanson, *Prog. Part. Nucl. Phys.* **93**, 143 (2017).
 - [3] H. X. Chen, W. Chen, X. Liu, and S. L. Zhu, *Phys. Rept.* **639**, 1 (2016).
 - [4] F. K. Guo, C. Hanhart, U. G. Meißner, Q. Wang, Q. Zhao, and B. S. Zou, *Rev. Mod. Phys.* **90**, 015004 (2018) [erratum: *Rev. Mod. Phys.* **94**, 029901 (2022)].
 - [5] Yu. S. Kalashnikova and A. V. Nefediev, *Phys. Usp.* **62**, 568 (2019).

- [6] Y. Yamaguchi, A. Hosaka, S. Takeuchi, and M. Takizawa, *J. Phys. G* **47**, 053001 (2020).
- [7] N. Brambilla, S. Eidelman, C. Hanhart, A. Nefediev, C. P. Shen, C. E. Thomas, A. Vairo and C. Z. Yuan, *Phys. Rept.* **873**, 1 (2020).
- [8] F. K. Guo, X. H. Liu, and S. Sakai, *Prog. Part. Nucl. Phys.* **112**, 103757 (2020).
- [9] H. X. Chen, W. Chen, X. Liu, Y. R. Liu, and S. L. Zhu, *Rept. Prog. Phys.* **86**, 026201 (2023).
- [10] E. Braaten and M. Lu, *Phys. Rev. D* **76**, 094028 (2007).
- [11] C. Hanhart, Yu. S. Kalashnikova, and A. V. Nefediev, *Phys. Rev. D* **81**, 094028 (2010).
- [12] A. A. Filin, A. Romanov, V. Baru, C. Hanhart, Yu. S. Kalashnikova, A. E. Kudryavtsev, U. G. Meißner, and A. V. Nefediev, *Phys. Rev. Lett.* **105**, 019101 (2010).
- [13] F. K. Guo and U. G. Meißner, *Phys. Rev. D* **84**, 014013 (2011).

⁵ That zeros in the T -matrix invalidate the original Weinberg formalism was discussed in Refs. [39, 45, 46].

- [14] R. Aaij *et al.* [LHCb], Nature Phys. **18**, 751 (2022).
- [15] R. Aaij *et al.* [LHCb], Nature Commun. **13**, 3351 (2022).
- [16] R. Blankenbecler, M. L. Goldberger, S. W. MacDowell, and S. B. Treiman, Phys. Rev. **123**, 692 (1961).
- [17] M. Doring, C. Hanhart, F. Huang, S. Krewald, and U. G. Meißner, Nucl. Phys. A **829**, 170 (2009).
- [18] R. Omnès, *Introduction to Particle Physics* (John Wiley & Sons Ltd, London, 1971).
- [19] M. Padmanath and S. Prelovsek, Phys. Rev. Lett. **129**, 032002 (2022).
- [20] S. Chen, C. Shi, Y. Chen, M. Gong, Z. Liu, W. Sun, and R. Zhang, Phys. Lett. B **833**, 137391 (2022).
- [21] Y. Lyu, S. Aoki, T. Doi, T. Hatsuda, Y. Ikeda, and J. Meng, [arXiv:2302.04505 [hep-lat]].
- [22] E. Braaten and J. Stapleton, Phys. Rev. D **81**, 014019 (2010).
- [23] V. Baru, X. K. Dong, M. L. Du, A. Filin, F. K. Guo, C. Hanhart, A. Nefediev, J. Nieves, and Q. Wang, Phys. Lett. B **833**, 137290 (2022).
- [24] A. B. Raposo and M. T. Hansen, PoS **LATTICE2022**, 051 (2023).
- [25] L. Meng and E. Epelbaum, JHEP **10**, 051 (2021).
- [26] V. Baru, A. A. Filin, C. Hanhart, Yu. S. Kalashnikova, A. E. Kudryavtsev, and A. V. Nefediev, Phys. Rev. D **84**, 074029 (2011).
- [27] M. Schmidt, M. Jansen, and H. W. Hammer, Phys. Rev. D **98**, 014032 (2018).
- [28] E. Braaten, L. P. He, and J. Jiang, Phys. Rev. D **103**, 036014 (2021).
- [29] M. L. Du, V. Baru, X. K. Dong, A. Filin, F. K. Guo, C. Hanhart, A. Nefediev, J. Nieves, and Q. Wang, Phys. Rev. D **105**, 014024 (2022).
- [30] V. Baru, E. Epelbaum, A. A. Filin, and J. Gegelia, Phys. Rev. C **92**, 014001 (2015).
- [31] V. Baru, E. Epelbaum, and A. A. Filin, Phys. Rev. C **94**, 014001 (2016).
- [32] J. Gasser and H. Leutwyler, Annals Phys. **158**, 142 (1984).
- [33] V. Baru, E. Epelbaum, A. A. Filin, C. Hanhart, U. G. Meißner, and A. V. Nefediev, Phys. Lett. B **726**, 537 (2013).
- [34] D. Becirevic and F. Sanfilippo, Phys. Lett. B **721**, 94 (2013).
- [35] K. W. McVoy, Nucl. Phys. A **115**, 481 (1968).
- [36] C. Hanhart, J. R. Pelaez, and G. Rios, Phys. Rev. Lett. **100**, 152001 (2008).
- [37] F. K. Guo, C. Hanhart, and U. G. Meißner, Eur. Phys. J. A **40**, 171 (2009).
- [38] C. Hanhart, J. R. Pelaez, and G. Rios, Phys. Lett. B **739**, 375 (2014).
- [39] S. Weinberg, Phys. Rev. **137**, B672 (1965).
- [40] D. Morgan, Nucl. Phys. A **543**, 632 (1992).
- [41] V. Baru, J. Haidenbauer, C. Hanhart, Y. Kalashnikova, and A. E. Kudryavtsev, Phys. Lett. B **586**, 53 (2004).
- [42] I. Matuschek, V. Baru, F. K. Guo, and C. Hanhart, Eur. Phys. J. A **57**, 101 (2021).
- [43] Y. Li, F. K. Guo, J. Y. Pang, and J. J. Wu, Phys. Rev. D **105**, L071502 (2022).
- [44] M. Albaladejo and J. Nieves, Eur. Phys. J. C **82**, 724 (2022).
- [45] V. Baru, C. Hanhart, Yu. S. Kalashnikova, A. E. Kudryavtsev, and A. V. Nefediev, Eur. Phys. J. A **44**, 93 (2010).
- [46] X. W. Kang and J. A. Oller, Eur. Phys. J. C **77**, 399 (2017).

Appendix A: Theoretical framework and fitting procedure

1. T -matrix

In the isospin limit, the contact potential up to next-to-leading order in the nonrelativistic expansion for the S -wave DD^* isoscalar ($I = 0$) state reads

$$V_C^{I=0}(k, k') = c_0 + c_2(k^2 + k'^2), \quad (\text{A1})$$

where c_0 and c_2 are the low-energy constants and k (k') is the 3-momentum of the incoming (outgoing) particle in the the center-of-mass (c.m.) frame. In the framework of the time-ordered-perturbation theory, the one-pion exchange (OPE) potential is written as

$$V_{\text{OPE}}^{I=0}(E, k, k') = \frac{g^2}{8f_\pi^2} \int_{-1}^1 dz D^\pi(E, k, k', z) \times (k^2 + k'^2 - 2kk'z), \quad (\text{A2})$$

where

$$D^\pi(E, k, k', z) = -\frac{D_1(E, k, k', z) + D_2(E, k, k', z)}{2\omega_\pi(q^2)},$$

with

$$D_1^{-1}(E, k, k', z) = 2M_D + \frac{k^2 + k'^2}{2M_D} + \omega_\pi(q^2) - E - i\epsilon,$$

$$D_2^{-1}(E, k, k', z) = 2M_{D^*} + \frac{k^2 + k'^2}{2M_{D^*}} + \omega_\pi(q^2) - E - i\epsilon,$$

and $\omega_\pi(q^2) = \sqrt{m_\pi^2 + k^2 + k'^2 - 2kk'z}$, that is, the pion is treated fully relativistically while the $D^{(*)}$ mesons are nonrelativistic.

The T -matrix (amplitude) is obtained as a solution of the Lippmann-Schwinger equation

$$T(E, k, k') = V(E, k, k') - \int \frac{d^3\mathbf{q}}{(2\pi)^3} V(E, k, q) G(E, q) T(E, q, k'), \quad (\text{A3})$$

where the potential is a sum of the contact term and OPE,

$$V(E, k, k') = V_C(k, k') + V_{\text{OPE}}(E, k, k'). \quad (\text{A4})$$

In order to render the integral in Eq. (A3) well defined, we set a sharp cutoff Λ . To arrive at the results in Fig. 4, Λ is chosen to be 500 MeV. The DD^* propagator is expressed as

$$G(E, q) = \left[M_{D^*} + M_D + \frac{q^2}{2\mu} - E - \frac{i}{2}\Gamma(E, q) \right]^{-1} \quad (\text{A5})$$

where $\mu = M_D M_{D^*} / (M_D + M_{D^*})$ is the reduced mass,

$$\Gamma(E, q) = \frac{g^2 M_D}{8\pi f_\pi^2 M_{D^*}} \left[\Sigma(s) - \Sigma_0(s) \theta(M_D + m_\pi - M_{D^*}) \right],$$

with $s = [E - M_D - q^2/(2\mu)]^2$, and

$$\Sigma(s) = \left[\frac{\lambda(s, M_D^2, m_\pi^2)}{2\sqrt{s}} \right]^{3/2}, \quad (\text{A6})$$

where $\lambda(a, b, c) = a^2 + b^2 + c^2 - 2ab - 2bc - 2ca$ is the Källén triangle function. Here

$$\begin{aligned} \Sigma_0(s) &= \Sigma(M_{D^*}^2) \\ &+ 2M_{D^*} \left(E - M_{D^*} - M_D - \frac{q^2}{2\mu} \right) \Sigma'(M_{D^*}^2), \end{aligned}$$

where the first and second terms renormalize the D^* mass and wave function, respectively, if $M_{D^*} < M_D + m_\pi$.

2. Chiral extrapolation of f_π and g

For convenience, we introduce the ratio $\xi = m_\pi/m_\pi^{\text{ph}}$ with m_π^{ph} the physical pion mass. For the masses of the D and D^* we stick to the values used in the lattice calculations and quoted explicitly in Ref. [19]. For the pion decay constant f_π , we resort to the result of the one-loop chiral perturbation theory [32] and cast it into the form [33]

$$f_\pi(\xi) = f_\pi^{\text{ph}} \left[1 + \left(1 - \frac{f_0}{f_\pi^{\text{ph}}} \right) (\xi^2 - 1) - \frac{(m_\pi^{\text{ph}})^2}{8\pi^2 f_0^2} \xi^2 \log \xi \right],$$

where $f_0 \equiv f_\pi(m_\pi = 0) = 85$ MeV [34] and $f_\pi^{\text{ph}} = 92.1$ MeV.

For the chiral extrapolation of the $DD^*\pi$ coupling g , we employ the lattice results of Ref. [34] and express it in terms of the physical value g^{ph} and $g_0 \equiv g(m_\pi = 0)$ as [33]

$$g(\xi) = g^{\text{ph}} [1 + C_1(\xi^2 - 1) + C_2 \xi^2 \log \xi], \quad (\text{A7})$$

where $g^{\text{ph}} = 0.57$ is determined from the experimentally measured $D^{*+} \rightarrow D^0 \pi^+$ decay width [29],

$$C_1 = 1 - \left[1 - \frac{1 + 2g_0^2}{8\pi^2 f_0^2} (m_\pi^{\text{ph}})^2 \log \frac{m_\pi^{\text{ph}}}{\mu_{\text{lat}}} + \alpha_{\text{lat}} (m_\pi^{\text{ph}})^2 \right]^{-1},$$

$$C_2 = -\frac{1 + 2g_0^2}{8\pi^2 f_0^2} (m_\pi^{\text{ph}})^2 (1 - C_1),$$

and the parameters take the values [34]

$$g_0 = 0.46, \quad \alpha_{\text{lat}} = -0.16 \text{ GeV}^{-2}, \quad \mu_{\text{lat}} = 1 \text{ GeV}.$$

3. Fitting procedure

In this appendix we describe the procedure employed to fit $p \cot \delta(p^2)$ extracted from the lattice data in Ref. [19] using the model described above which explicitly takes into account the OPE interaction.

In particular, the function $p \cot \delta(p^2)$ is related to the DD^* S -wave on-shell scattering T -matrix $T(E)$ as

$$p \cot \delta(p^2) = -\frac{2\pi}{\mu} T^{-1}(E) + ip, \quad (\text{A8})$$

where $T(E) \equiv T(M_D + M_{D^*} + p^2/(2\mu), p, p)$ is a solution of the Lippmann-Schwinger equation (A3).

Since the lattice data points for $p \cot \delta(p^2)$ are extracted using the Lüscher method, their uncertainties have non-Gaussian shapes, which prevents us from performing a naive χ^2 fit. Instead, we employ the probability distribution extracted for each lattice data point from Ref. [19] and generate 1000 sets of quasi-data points according to these distributions. Each generated set (with 3 or 4 data points depending on the fit) is then fitted with our model by minimizing

$$\chi^2 = \sum_i \left(p_i \cot \delta(p_i^2) \Big|_{\text{model}} - p_i \cot \delta(p_i^2) \Big|_{\text{quasi-data}} \right)^2$$

as a function of the parameters c_0 and c_2 , where i enumerates the data points used in the fit—see the main text for the details of the selection procedure of the data points. The resulting 1000 pairs $\{c_0, c_2\}$ are used then to evaluate the most probable values of these low-energy constants, $p \cot \delta(p^2)$, and the corresponding 68% confidence intervals.

Appendix B: Analysis of the lattice data for the smaller charm quark masses

In this appendix we provide the fit results for the lattice data from Ref. [19] corresponding to the smaller charm quark masses, namely

$$M_D = 1762 \text{ MeV}, \quad M_{D^*} = 1898 \text{ MeV}, \quad (\text{B1})$$

while the pion mass remains the same as before, $m_\pi = 280$ MeV. The obtained 3- and 4-point fits are shown in Fig. 5. In these settings, the lhc position corresponds to $(p/E_{DD^*})^2 = -0.0011$. As stated in the main text, these fits demonstrate essentially the same behaviour as those shown in Fig. 4 and as such lead to the same conclusions.

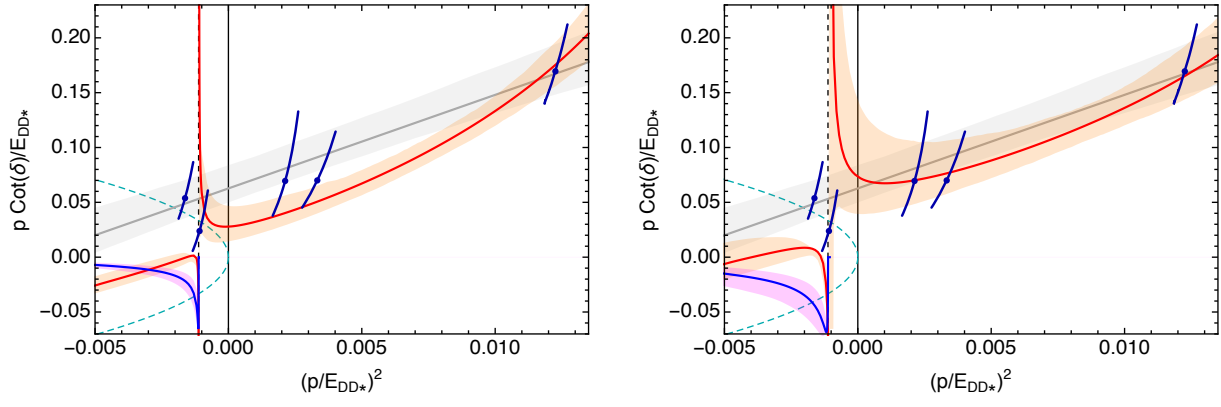


FIG. 5. Fits for the alternative set of parameters provided in Ref. [19] and quoted in Eq. (B1). See the caption of Fig. 4 for the details.